

Spectroscopic monitoring of the Herbig Ae star HD 104237 [★]

II. Non-radial pulsations, mode analysis and fundamental stellar parameters

A. Fumel^{1,2} and T. Böhm^{1,2}

¹ Université de Toulouse; UPS-OMP; IRAP; Toulouse, France
e-mail: aurelie.fumel@ast.obs-mip.fr, boehm@obs-mip.fr
² CNRS; IRAP; 14, avenue Edouard Belin, F-31400 Toulouse, France

Received August 3rd, 2011; accepted XX, 2011

ABSTRACT

Context. Herbig Ae/Be stars are intermediate-mass pre-main sequence (PMS) stars showing signs of intense activity and strong stellar winds, whose origin is not yet understood in the frame of current theoretical models of stellar evolution for young stars. The evolutionary tracks of the earlier Herbig Ae stars cross for a significant fraction of their evolution towards the main sequence the theoretical PMS instability strip located roughly in the same area of the HR diagram as the δ Scuti variables. Many of these stars exhibit pulsations of δ Scuti type.

Aims. We carry out a thorough analysis of the line profile variations of the pulsating prototype Herbig Ae star HD 104237 based on high-resolution spectroscopical time-series, identify the dominant non-radial pulsation mode, and perform the most accurate determination of its fundamental parameters in preparation of an asteroseismic modeling.

Methods. HD 104237 is a pulsating Herbig Ae star with eight detected frequencies based on the analysis of radial velocity variations. In this article, we reinvestigated an extensive high-resolution quasi-continuous spectroscopic data set in order to search for very faint indications of non-radial pulsations in the line profile. To do this, we worked on dynamical spectra of equivalent photospheric (LSD) profiles of HD 104237. A 2D Fourier analysis (F2D) was performed of the entire profile and enabled the identification of the dominant non-radial pulsating mode. The temporal variation of the central depth of the line was studied with the time-series analysis tools *Period04* and *SigSpec*. The development of a highly accurate continuum normalization method enabled us to determine reliably the equivalent width of chosen absorption lines and to perform a new determination of the fundamental stellar parameters.

Results. Following the previous studies on this star, our analysis of the dynamical spectrum of recentered LSD profiles corresponding to the 22nd – 25th of April 1999 nights spectra has confirmed the presence of multiple oscillation modes of low-degree ℓ in HD 104237 and led to the first direct detection of a non-radial pulsation mode in this star: the dominant mode $F1$ was identified by the Fourier 2D method having a degree ℓ value comprised between 1 and 2, the symmetry of the pattern variation indicating an azimuthal order of ± 1 . The detailed study of the fundamental stellar parameters has provided a T_{eff} , $\log g$ and iron abundance of 8550 ± 150 K, 3.9 ± 0.3 and -4.38 ± 0.19 (i.e. $[\text{Fe}/\text{H}] = +0.16 \pm 0.19$), respectively.

Key words. stars: pre-main-sequence – stars: oscillations – stars: individual: HD 104237 – stars: binaries: spectroscopic – stars: fundamental parameters –

1. Introduction

Pre-main sequence (PMS) stars of intermediate mass (2 to 10 M_{\odot}) are known as Herbig Ae/Be (hereafter HAeBe) stars, following a first classification by Herbig (1960). As their name indicates, they are of spectral type A or B and luminosity classes III to V (for a review, see Waters & Waelkens 1998). Their Spectral Energy Distribution (SED) is characterized by infrared (IR) excess and ultraviolet (UV) extinction mainly due to thermal re-emission from UV to IR of a circumstellar (CS) dust shell or disk (or both), making the photometric assessment of spectral types and stellar temperatures of these stars rather uncertain.

HAeBe stars show signs of intense stellar activity, variability and winds. Indeed, the frequently observed emission in Mg II h and k lines, Ca II IR triplet, Ca II H and K line, He I 5876 Å, many Fe II lines, Na I D, N V, Si IV and C IV resonance lines, imply the high temperature of a chromosphere or corona to be formed. Short-term variability of many of these

lines are observed and P Cygni profiles of H α , H β , Mg II h and k lines present in the spectra of some of these stars indicate the presence of strong and structured stellar winds (see e.g. Praderie et al. 1982, 1986; Catala & Talavera 1984; Catala et al. 1986a,b; Catala & Kunasz 1987; Catala 1988; Catala et al. 1993; Böhm & Catala 1995; Böhm et al. 1996).

A wide-spread idea consists in invoking magnetism as being responsible for such active stellar phenomena, requiring either the presence of a primordial magnetic field or a dynamo mechanism whose basic ingredients are classically convection and rotation. On one hand, recent spectropolarimetric observations of Herbig stars indicate the presence of significant magnetic fields only in a small 10% fraction of them (Wade et al. 2007), these results being in agreement with the primordial fossil field hypothesis. On the other hand, considering a possible dynamo mechanism, the position of HAeBe stars in the HR diagram indicates that they are in the radiative phase of their quasi-static contraction towards the main sequence (Iben 1965; Gilliland 1986). Therefore, in absence of subphotospheric convection, a classical solar-type magnetic dynamo mechanism can not be at work.

[★] Based on observations collected at the 1.9m SAAO Radcliffe telescope

The HAeBe stars activity remains therefore quite paradoxical in the frame of current theoretical evolutionary models for PMS stars, although there exist some approaches to understand its origin. As possible explanations, Palla & Stahler (1990) suggested that outer convection zone could be induced by deuterium burning. Vigneron et al. (1990) proposed the internal rotation as energy source, the friction exerted at the stellar surface by the angular momentum losses creating a non-convective turbulent layer, responsible for a dynamo effect; this model was later refined by Lignieres et al. (1996).

An external origin, involving an accretion disk dissipating gravitational energy into a boundary layer at the stellar surface, was invoked by Bertout et al. (1988) to explain activity in classical T Tauri stars, T Tauri stars being the lower mass PMS counterparts to HAeBes. However, Böhm & Catala (1995) showed that the energy flux emitted in winds and some activity tracers seems to increase with effective temperature, which is in favor of an internal activity source rather than a CS origin. Thus, as of today, growing evidences tend to indicate that the energy needed to produce this activity might be of internal stellar origin, but no definite answer has been provided. It is a major concern for testing young stellar evolutionary theory to solve this still open question about HAeBe stellar activity, by constraining the internal structure of these objects using asteroseismic techniques, i.e. the analysis and modeling of stellar pulsations, if observed.

Photometric and spectroscopic variability have indeed been observed in HAeBe stars, on very different time scales (from minutes to years). Large and irregular photometric variations ($\geq 0^m.5$) with time scales from weeks to years are thought to be due to variable obscuration by CS patchy dust clouds, particularly strongly in the younger objects (van den Ancker et al. 1998). Variations of the order of a tenth of magnitude (mag) in amplitude, with time scales of hours to days, can be explained as due to clumpy accretion (van den Ancker et al. 1998 and references therein) or due to chromospheric activity, including winds, modulated by the star's rotation (Catala et al. 1999). Stellar pulsations, which are here the subject of our interest, induce typically a millimagnitude (mmag) photometrical variability with time scales of minutes to hours.

The existence of such stellar pulsations in HAeBe stars are known since Breger (1972) discovered two pulsating candidates, V588 Mon and V589 Mon, in the young open cluster NGC 2264. Subsequently, two additional pulsating Herbig stars were detected: HR 5999 (Kurtz & Marang 1995) and HD 104237 (Donati et al. 1997). Motivated by these detections, Marconi & Palla (1998) investigated theoretically a PMS instability strip for the first three radial modes of pulsations and concluded on a topology of this instability strip, corresponding roughly to the same area in the HR diagram as the δ Scuti variables. The study of Marconi & Palla (1998) showed that most of the Herbig Ae stars are expected to cross it for a significant fraction of their evolution to the main sequence (5 to 10% of their PMS phase). Since the precise location and boundaries of the PSM instability strip has not yet been observationally constrained, it is necessary to identify and study the largest number of PMS pulsating objects, giving priority to multiperiodic pulsators which are suitable and promising candidates for future asteroseismic modeling, and, by this mean, supplying constraints on theoretical evolutionary pre-main sequence models.

As of today, a significant number of Herbig Ae stars, either field stars or members of young open clusters, have indeed revealed to be pulsating at timescale typical of δ Scuti stars, i.e. with short periods (from ≈ 20 min to several hours) and small amplitudes (from mmag to few hundredths of mag in case of pho-

tometry, and less than typically $1 - 2 \text{ km s}^{-1}$ for radial velocity studies) (for reviews see e.g. Catala 2003; Marconi & Palla 2004; Zwintz et al. 2004; Zwintz 2008). Most of them have been studied in photometry, but only very few in spectroscopy (e.g. Böhm et al. 2004, 2009). However, due to cancellation effects, only modes of low degree are detected in photometry or from radial velocity curves. Therefore, high-resolution spectroscopy is necessary to study the weak variations induced by non-radial pulsations in the rotationally-broadened photospheric line profiles, and thus to carry out a comprehensive pulsational analysis in preparation for seismic modeling. It should be noted that binarity is common amongst HAeBe stars with approximately 60% (Baines et al. 2006). As we will see in Sect. 2, HD 104237 is also a spectroscopic binary, which complicates tremendously the analysis of its spectrum.

This article is the second of a series on the prototype Herbig Ae star HD 104237, starting with the article by Böhm et al. (2004). The first article presented the detection of multiperiodic oscillations in the radial velocity curves of the star and the analysis of its binary orbit, amongst others. In this present article, we describe the direct search and detection of oscillations in the line profiles, the mode identification of the dominant non-radial pulsation mode, as well as a fundamental stellar parameter determination by spectroscopic means. This work represents therefore the basis for the asteroseismic modeling we will present in a forthcoming article (Fumel et al. 2011).

The article is structured as follows: in Sect. 2, we review in detail previous works on HD 104237, Sect. 3 sums up the spectroscopic observations we worked with and data reduction, Sect. 4 presents our detection and identification of non-radial pulsations in HD 104237, Sect. 5 describes the spectral continuum determination tool we have developed to obtain optimized high-quality spectra, in Sect. 6 we detail the fundamental parameter determination of HD 104237 we carried out and finally we conclude and discuss our results in Sect. 7.

2. Previous works on HD 104237

Hu et al. (1989, 1991) derived from photometric and spectroscopic studies that HD 104237, or DX Cha, is a member of the Herbig Ae/Be group. Moreover, it is a prototype of this group of stars and a particularly suitable target since it is very bright ($m_v = 6.6$), which enables to observe it in high resolution spectroscopic mode. It is located in the ϵ Chamaeleontis young stellar group at a *Hipparcos* distance of $116 \pm 8 \text{ pc}$ (van den Ancker et al. 1997). HD 104237 is actually a multiple system whose primary component (hereafter simply called HD 104237 or the "primary") is a Herbig Ae star with several low-mass companions at separations between $1''$ and $15''$ (Feigelson et al. 2003), including a close K3 companion in an eccentric 19.9-day orbit (hereafter HD 104237b or the "secondary"). This very close component of approximate spectral class K3 forms with the primary a spectroscopic binary (Böhm et al. 2004). Indeed, K3-type spectral features (including Li I 6707 Å and Ca I 6718 Å lines) are observed in the primary spectra (Feigelson et al. 2003), that makes its spectroscopic analysis trickier since one has to take into account the pollution generated by the faint secondary component in the dominant primary spectrum.

2.1. Previous fundamental parameter determination

The strong IR excesses and the UV-extinction due to the presence of CS dust, the emission components in many absorption lines, the P Cygni profiles observed notably in the Balmer lines and the spectroscopic binary pollution make the determination of most fundamental stellar parameters of HD 104237 difficult. Thus, the spectral types available in the literature for HD 104237 range from A0 to A8 (implying a large range in possible T_{eff} values) and its bolometric luminosity from ≈ 20 to $60 L_{\odot}$. The associated stellar parameters such as the mass and the age of the star can be estimated from temperature and luminosity with stellar evolutionary models. They rely therefore strongly both on the accuracy of the location of the star in the HR diagram and on the adopted evolutionary models and are also not precisely determined, as well as all the parameters that result from them (e.g. $\log g$). The most important parameters of HD 104237 (primary and secondary) found in the literature are chronologically summarized in Table 1 and are detailed below.

Hu et al. (1989) based their first determination of a A0Vpe spectral type on the absorption profiles of the Balmer lines and the strong Ca II K line (3933.7 Å). Subsequently, the presence of emission components in the H α and H β was understood to be misleading the determination of the spectral type. In a second article Hu et al. (1991) therefore derived an A4Ve spectral type from UV absorption lines. From an integrated radiant flux (0.1 to $10 \mu\text{m}$) of $8.62 \times 10^{-8} \text{ erg cm}^{-2} \text{ s}^{-1}$ and a distance of 88 pc they inferred a $\log (L_{\star}/L_{\odot})$ of 1.34. Using the dwarf temperature scale of Schmidt-Kaler (1982), they converted this spectral type to a T_{eff} of 8450 K from which they obtained a stellar radius of $2.2 R_{\odot}$. Brown et al. (1997) carried out a study of the hot disk wind of HD 104237 by means of UV spectra and assumed it to be of spectral type A7IVe. Using the accurate absolute astrometric and photometric data yielded by the Hipparcos satellite, van den Ancker et al. (1997) computed new T_{eff} , $\log (L_{\star}/L_{\odot})$, mass and age values for HD 104237 (cf. Table 1). Although their method included corrections taking into account the fact that HAe/Be stars often exhibit anomalous extinction law for their circumstellar material and UV spectra often lead to overestimation of temperatures due to the presence of heated layers in the immediate surrounding of the star's photosphere, they used as a spectral type the non-corrected result of Hu et al. (1989) based on optical spectra, whose many lines are polluted by emission components. In a next article van den Ancker et al. (1998) proposed a cooler spectral type (A4IVe), in agreement with Hu et al. (1991), and derived corresponding new parameters. The uncertainties on the effective temperature were estimated values and not determined in a statistical procedure.

In their investigation of the environment of HD 104237, Grady et al. (2004) derived a new spectral type of A7.5-A8Ve based on the comparison between FUV and UV spectra of HD 104237 and others stars with well-known spectral types. Again, the error bars on the spectral type were empirically determined. This cooler spectral type, close to the determination of Brown et al. (1997), and the $\log (L_{\star}/L_{\odot})$ derived by the authors led to an age of 5 Myr, which is noticeably greater than the previous age estimations (van den Ancker et al. 1997, 1998; Feigelson et al. 2003) but closer to the ages of the HD 104237 quintet low-mass members (Feigelson et al. 2003). Using evolutionary tracks and isochrones from Palla & Stahler (2001) and both the stellar parameters from van den Ancker et al. (1998) and Grady et al. (2004), Böhm et al. (2004) concluded on an age of 2 Myr for HD 104237, in agreement with van den Ancker et al. (1997, 1998) and Feigelson et al. (2003),

and independently concluded on a similar value of the stellar mass $M_{\star} = 2.2 \pm 0.1 M_{\odot}$ as previous studies. Moreover they calculated a mass ratio M_P/M_S of 1.29 ± 0.02 , based on measures of the primary and secondary radial velocities with respect to the systemic velocity of the binary system, that enabled them to estimate the mass of the secondary to be of $1.7 \pm 0.1 M_{\odot}$. Assuming the same age for both components, they confirmed a K3 spectral type for the secondary and assessed a temperature of about 4750 K and a luminosity of one tenth of L_P . Starting from the spectral type proposed by Grady et al. (2004), Luhman (2004) computed a new T_{eff} (with Schmidt-Kaler 1982 temperature scale) and $\log (L_{\star}/L_{\odot})$ (from *I*-band magnitudes). Placing these new parameters in a HR diagram with evolutionary tracks from Palla & Stahler (1999) enabled Luhman (2004) to confirm an age of about 2 Myr. Finally, based on low-resolution spectra and going by the fact that the strengths of Ca II and H δ lines undergo a reverse relationship with temperature, Lyo et al. (2008) managed to constrain the spectral type of HD 104237, even in case of contamination by emission of these lines. Since they obtain a spectral type of A4 from the Ca II line and A5 from the H δ line, they adopted a spectral type of A4/A5 for this star.

Acke & Waelkens (2004) used the T_{eff} and $\log g$ presented in Meeus et al. (2001) (and references therein) to carry out a chemical analysis of several PMS stars including HD 104237. They measured the equivalent widths of many chemical elements and converted them to abundances using the program MOOG (Sneden 1973), but taking into account neither the binarity of this star (which adds a continuum veiling along with additional lines from the secondary) nor the asymmetries or the emission components in the line profiles. Using the solar abundances by Anders & Grevesse (1989) they found a solar-like global metallicity ($[M/H] = +0.06 \pm 0.05$) and a solar abundances for several chemical elements including Fe ($[Fe/H] = +0.09 \pm 0.19$) where $[Fe/H] = \log \left(\frac{N_{\text{Fe}}}{N_{\text{H}}} \right)_{\text{HD 104237}} - \log \left(\frac{N_{\text{Fe}}}{N_{\text{H}}} \right)_{\odot}$.

Donati et al. (1997) measured a $v \sin i$ of $12 \pm 2 \text{ km s}^{-1}$, which suggests either that HD 104237 is viewed close to pole-on or that it is a moderate rotator. Grady et al. (2004) found indeed an inclination of the stellar rotation axis of 18^{+14}_{-11} , which implies an equatorial velocity of 38 km s^{-1} . Böhm et al. (2006) detected a modulation of the H α line profile with a period of $100 \pm 5 \text{ hrs}$ and suggested a rotational origin, yielding a similar inclination of 23^{+9}_{-8} . This value of P_{rot} was confirmed by Testa et al. (2008) in a X-ray study of the HD 104237 system.

Concerning magnetism, Donati et al. (1997) detected a weak field of about 50 G in HD 104237, but a later survey by Wade et al. (2007) could not confirm it at this stage.

As can be seen from all the different contributions cited here-above, no in-depth spectral type determination has been done as of today: indeed, all determinations were based either on photometry or on low-resolution spectroscopy (except the rough estimate by Donati et al. 1997), and a thorough redetermination of fundamental parameters based on high-resolution spectroscopy is required for an independent conclusion. This is one of the major goals of the work presented in this article in Sect. 6 and a basic requirement for a subsequent asteroseismic modeling (Fumel et al. 2011), but also in order to precise the PMS instability strip features and boundaries. Knowing these parameters will eventually allow us to better understand the origin of the activity observed in the Herbig Ae/Be stars and test the current theoretical evolutionary models for PMS stars.

Table 1. Stellar parameters of HD 104237. 2nd column: P corresponds to the stellar parameters of the primary and S to those of the secondary. Values in italics ($\log g$ and R/R_\odot): computed from universal gravitation and Stefan-Boltzmann laws. References: [1] Hu et al. (1989), [2] Hu et al. (1991), [3] Brown et al. (1997), [4] van den Ancker et al. (1997), [5] Donati et al. (1997), [6] van den Ancker et al. (1998), [7] Grady et al. (2004), [8] Böhm et al. (2004), [9] Luhman (2004), [10] Acke & Waelkens (2004), [11] Lyo et al. (2008), [12] Böhm et al. (2006). Mass and ages are determined using the model isochrones and isomass of: ^(a) Iben & Renzini (1984), ^(b) Palla & Stahler (1993), ^(c) Siess et al. (2000), ^(d) Palla & Stahler (1999), ^(e) Palla & Stahler (2001).

Ref.		Sp. Type	$\log T_{\text{eff}}$	T_{eff} (K)	$\log (L_\star/L_\odot)$	$\log g$	M_\star/M_\odot	R_\star/R_\odot	Age (Myr)	$v \sin i$ (km.s ⁻¹)	i (°)
[1]	P	A0Vpe									
[2]	P	A4Ve	3.93	8450	1.34	4.1	2.1 ^(a)	2.2			
[3]	P	A7IVe									
[4]	P	A0Vpe [1]	3.98 ± 0.05	9550^{+550}	1.77 ± 0.06	3.9	$2.5 \pm 0.1^{(b)}$	2.9	$2.0 \pm 0.5^{(b)}$		
[5]	P	A4V								12 ± 2	
[6]	P	A4IVe+sh	3.93 ± 0.05	8500^{+500}	$1.55^{+0.06}_{-0.05}$	3.9	2.3 ^(b)	2.8	2.0 ^(b)		
[7]	P	A7.5-8Ve	3.86	≈ 7300	$1.42^{+0.04}_{-0.07}$	3.7	2.1 ^(c)	3.3	5 ^(c)		18^{+14}_{-11}
[8]	P	A7.5-8Ve [7]		≈ 7300 [7]	1.42 [7]	3.7	$2.2 \pm 0.1^{(e)}$	3.3	2 ^(e)		
	S	K3	3.675	4730	0.42	3.9	$1.7 \pm 0.1^{(e)}$	2.5	2 ^(e)		
[9]	P	A7.75 [7]	3.88	7648	1.46	3.8	2.2 ^(d)	3.1	$\approx 2^{(d)}$		
[10]	P		3.90	8000		4.5				10 ± 1	
[11]	P	A4-5Ve									
[12]	P										23^{+9}_{-8}

2.2. Previous pulsational analysis

The primary component of the HD 104237 system has revealed being a pulsating Herbig Ae star. From spectropolarimetric observations of active stars including HD 104237, Donati et al. (1997) detected for the first time radial velocity variations in equivalent photospheric LSD (cf. Sect. 3) Stokes I spectra of this star and determined a period of 37.3 min. This short period was incompatible with a rotational modulation or a secondary companion and was attributed to stellar pulsations. This pulsational variability, typical of δ Scuti-type variables, was confirmed with photometric measurements by Kurtz & Müller (1999) who detected two frequencies. They computed the ratio of radial velocity to V light amplitude and found values typical for a δ Scuti star. Moreover, they calculated a value for the pulsation constant Q lower than the typical values given by the fundamental, the first and the second overtone in δ Scuti stars, indicating pulsations of higher overtone.

Böhm et al. (2004) obtained in 1999 and 2000 an extensive high-resolution ($R \approx 35000$) spectroscopic data set of HD 104237 at the 1.9m Radcliffe telescope of the SAAO (see Sect. 3). The resulting high quality radial velocity curve allowed them to detect for the first time by spectroscopic means multi-periodic oscillations in a PMS star (8 frequencies in the 1999 data set and 5 in the 2000 data set). Five frequencies of 1999 were identified with frequencies of 2000, between 28.50 and 35.60 d⁻¹. No pulsation was detected in HD 104237b in the night around the periastron, when both components are well separated in velocity, a result which is not astonishing given the position of the star in the HR diagram. The frequency differences of the 8, respectively 5 frequencies detected by Böhm et al. (2004) were smaller than the estimated large separation ($\Delta\nu_0 \approx 40 - 45 \mu\text{Hz}$), leading the authors to conclude on the nonradial nature of at least some of the pulsation modes detected in their work. More generally, no regular frequency pattern has been clearly identified in the pulsational behaviour of HD 104237. Böhm et al. (2004) pointed out (based on the frequency separation) the potential existence of 1 to 3 radial pulsation modes among the 5 frequencies observed both in 1999 and 2000, but at this time no clear mode identification in HD 104237 could have been performed for none of the modes. Since this first article was restricted to the analysis of radial velocity variations, we wanted to go a step further, and

reanalysed the spectral line profiles themselves in the same data set; the result of this study is presented thereafter.

The previously determined pulsation characteristics are summarized in Table 2. The three last frequencies of 1999 from Böhm et al. (2004) (f_6 to f_8) are included, although these authors considered them as less certain.

Using the results of Böhm et al. (2004), Dupret et al. (2006, 2007) found in a preliminary seismic modeling of HD 104237 that it is difficult to properly fit the observed frequencies with theoretical frequencies computed from models with T_{eff} and $\log(L/L_\odot)$ presented in van den Ancker et al. (1998) and Grady et al. (2004). An important result was their conclusion that HD 104237 is in fact not a typical δ Scuti type pulsator. Indeed, the p modes order corresponding to the observed frequencies are too high to be excited by the standard excitation mechanism of δ Scuti type variables, namely a κ -driving in the He II partial ionization zone. Such a modeling requires a precise knowledge of the stellar fundamental parameters which enter the evolution and oscillation codes and a good idea of ℓ and m for each observed mode. However, both are poorly known or not known at all in the case of HD 104237. In order to go further in this seismic study and to better constrain the internal structure of HD 104237, we will propose a more thorough and complete modeling of HD 104237 in a forthcoming article (Fumel et al. 2011), using the accurate stellar parameters determination as well as the pulsational information described in the present article.

3. SAAO spectroscopic observations and data reduction

The analysis presented in this article is based on parts of the data set described in Böhm et al. (2004), namely the high-resolution spectroscopic observations obtained in April 1999 and April 2000 at the 1.9 m SAAO (South African Astronomical Observatory) Radcliff telescope; all data were obtained with the GIRAFFE fiber-fed echelle spectrograph with a resolving power of about $R \approx 35000$.

HD 104237 was monitored in quasi-continuous mode throughout all the nights of the 1999 and 2000 runs (resp. 7 and 14 nights) in order to obtain high-resolution spectroscopic

Table 2. Previous pulsational analysis results for HD 104237. Col. 5: references: (1) Donati et al. (1997), (2) Kurtz & Müller (1999), (3) Böhm et al. (2004).

Year of observation	Frequency (d ⁻¹)	Period (min)	Amplitude	Ref.
1993	$f_1 = 37.3$	38.6 ± 1	0.65 km s^{-1}	(1)
1995	$f_1 = 39.6$	36.4 ± 1	0.65 km s^{-1}	(1)
1998	$f_1 = 33.29$ $f_2 = 36.61$	43.3 39.3	$11.2 \pm 0.5 \text{ mmag}$ $3.4 \pm 0.5 \text{ mmag}$	(2)
1999	$f_1 = 33.289$ $f_2 = 35.606$ $f_3 = 28.503$ $f_4 = 30.954$ $f_5 = 33.862$ $f_6 = 32.616$ $f_7 = 34.88$ $f_8 = 35.28$	43.257 40.443 50.521 46.521 42.525 44.150 41.28 40.82	1.320 km s^{-1} 0.474 km s^{-1} 0.195 km s^{-1} 0.139 km s^{-1} 0.099 km s^{-1} 0.105 km s^{-1} 0.1 km s^{-1} 0.05 km s^{-1}	(3)
2000	$f_1 = 35.609$ $f_2 = 33.283$ $f_3 = 31.012$ $f_4 = 28.521$ $f_5 = 32.375$	40.439 43.265 46.434 50.489 44.479	0.328 km s^{-1} 0.258 km s^{-1} 0.177 km s^{-1} 0.165 km s^{-1} 0.113 km s^{-1}	(3)

time-series necessary for an asteroseismic analysis. The covered wavelength domain usually was 426–688 nm (spread over 50 orders) in 1999 and 436–688 nm (spread over 47 orders) in 2000. In order to sample properly the previously known main pulsation period of about 40 minutes, subexposure times of 5 minutes were needed, yielding about 8 spectra per pulsation period, the brightness of HD 104237 enabling such short exposure times. A standard calibration strategy was applied. Values of Signal to Noise Ratios (SNR) per pixel at 550 nm ranged from 30 to 120 in 1999 and from 30 to 110 in 2000, with typical values of 50–70. Most of the data reduction was carried out following standard reduction procedures using the “ESPRIT” spectroscopic reduction package (Donati et al. 1997). Moreover, as the analysis of pulsations by high-resolution spectroscopy requires significant SNR, the least-square deconvolution (LSD) method as described in Donati et al. (1997) was applied. This method makes use of the multiplex gain of more than 500 lines present in the spectrum of this star, providing a high SNR equivalent photospheric profile. More precisely, it assumes that the local profile of all selected spectral lines is similar in shape (with different individual central depths), the line parameters being extracted from an appropriate catalogue, corresponding as close as possible to the fundamental parameters of the star of interest known at this stage of data reduction as A4-type (based on the results announced in Donati et al. 1997). In a subsequent step, the more than 100 narrow telluric vapor lines present in the spectra yielded the necessary multiplex information for a high precision radial velocity correction. All spectra were shifted to the heliocentric rest wavelength, and calibrated to a final intrinsic precision estimated to be around 100 ms^{-1} for this data set. In addition, HJD (Heliocentric Julian Date) have been calculated for each LSD profile. Details of observations and data reduction are thoroughly described in Böhm et al. (2004).

The detection and identification of non-radial pulsations described in Sect. 4 has been carried out on the data collected during the SAAO observing run in 1999, where we especially concentrated our study on the data of the nights from 22nd to 26th of April, these nights having yielded the longest individual time coverages. During the night of April 25th 156 high-resolution spectra were obtained during 10.9 hrs.

The fundamental parameter determination described in Sect. 6 has been performed on data collected during the night of 12th of April 2000 at SAAO; on this date, the eccentric binary orbit with a period of 19.859 days (see Böhm et al. 2004) separates during periastron both spectra with a relative shift of 60 km s^{-1} , thus avoiding at maximum pollution of the primary spectrum by the much fainter secondary companion HD 104237b.

The log of the observations we worked with are summarized in Table 3.

Table 3. Log of the observations we worked with.

Date	Time series duration (hrs)	Number of spectra	SNR (pixel ⁻¹) at 550 nm
22 Apr. 1999	8.2	74	55–120
23 Apr. 1999	10.2	91	40–90
24 Apr. 1999	10.8	136	30–100
25 Apr. 1999	10.9	156	30–60
26 Apr. 1999	7.7	58	30–80
12 Apr. 2000	3.6	35	40–60

4. Detection and identification of non-radial pulsations

Stellar pulsations are characterized by their frequencies and corresponding modes, specified by three quantum numbers: the order n , related to the number of radial nodes, the degree of the mode ℓ , indicating the total number of surface nodes, and the azimuthal order of the mode m such that $m = -\ell, -\ell + 1, \dots, \ell - 1, \ell$, where $|m|$ corresponds to the number of meridian nodes, i.e. showing nodal lines perpendicular to the stellar equator. Radial modes are characterized by $\ell = m = 0$ and non-radial modes by $\ell \neq 0$. Because of cancellation effects, photometry or radial velocity measurements are not able to access higher degrees of non-radial pulsations with typically $\ell \geq 3$ (Kennelly et al. 1996). The only direct way to investigate modes of higher degrees consists in analysing line-profile variations of rotationally-broadened photospheric profiles, where the 3D velocity field of the oscillating stellar surface induces profile variations due to Doppler effect (Vogt & Penrod 1983). The maximum attainable degree ℓ is increasing with the ratio $v \sin i$ to resolved spectral element ($\Delta v = c/R$, with R being the resolution of the spectrograph). This also implies that fast rotators seen almost pole-on only allow mode detection limited to low degrees, due to a lack of line profile width.

As explained in previous Section, we concentrated our study on the data of the 22nd–26th of April 1999. The initial work by Böhm et al. 2004 did not reveal any non-radial pulsation at first sight in the line profiles and these authors therefore decided to concentrate on radial velocity variations, also due to the fact that the star is a moderate rotator, seen 3/4 pole on and exhibiting a small $v \sin i$ of only $12 \pm 2 \text{ km s}^{-1}$. However, line profiles of this star are broadened in the wings by some additional agent, leading to a total width of almost 50 km s^{-1} , the double of the pure rotational broadening. The resolution of the GIRAFFE spectrograph at SAAO being of the order of $R \approx 35000$, a resolved element corresponds roughly to 8 km s^{-1} . This implies that a search for non radial pulsations (NRP) in this instrumental context is limited in this star to degrees ℓ of the order of 2 to 3, higher degrees being not observable due to a lack of rotational velocity resolution. In the present work we decided nevertheless to go one step further, and to reanalyse in depth the profile variations

themselves, not limiting the study to radial velocity variations. To do so, and in order to search for faint traces of non-radial pulsations in the primary component, each LSD profile has been corrected for its radial velocity. This correction comprises orbital motion, but also centroid shifts mainly due to radial pulsations. After recentering, a mean LSD profile, averaged over the whole run, has been subtracted from every profile in order to search for very faint signatures. This allowed us to detect line profile variations clearly indicative of non-radial stellar pulsations, inducing differential amplitudes of the order of 1.5% of the continuum. Also, it is obvious from the differential dynamical spectra of Fig. 1 that beating between nearby frequencies occur, which leads to the conclusion that probably more than one NRP must be acting (the night of April 26th is not represented due to shorter coverage). The sampling of the LSD profiles in dispersion direction satisfies the Nyquist criteria, i.e. one resolved element projects on 2 velocity bins of 4 km s^{-1} each. Fig. 2 shows the differential amplitude variations at line center, extracted by taking the median value of the 3 central velocity bins of each spectrum.

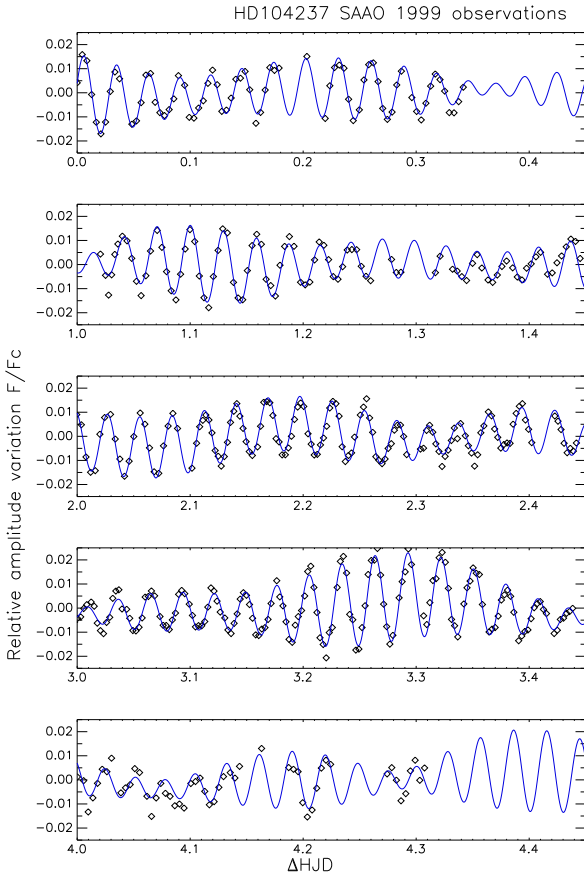


Fig. 2. Amplitude variation of the central velocity bins of the residual LSD profile of the nights of Apr. 22nd to 26th 1999. Superimposed is a fit of the data corresponding to the result of the frequency analysis as presented in Tab. 4.

4.1. Central profile analysis with SigSpec and Period04

We choose to carry out a frequency analysis of our LSD residual profiles time-series using the *Period04* package (Lenz & Breger 2005) in parallel with the *Sigspec* package (Reegen 2007). They both use, in iterative process, combination of Discrete Fourier Transform (DFT) and least-squares fitting algorithms to extract

the frequencies, amplitudes and phases of multi-periodic signals in not-equally spaced data sets. Both process fit simultaneously all the frequencies, amplitudes and phases detected so far when a new peak is found in the DFT spectrum of the time-series. Unlike *Period04* which provides a flexible interface to perform multiple-frequency fits, *Sigspec* is fully automatic. In addition, it includes a rigorous statistical treatment of how to compute the significance level of these peaks (with respect to white noise) and provides directly a significance parameters, the spectral significance *sig*. In order to avoid at maximum low frequency night-to-night variations, we corrected our central velocity bin time series by subtracting a nightly average. Still, by doing so, some low frequencies persisted as can be seen later on.

The results of the *Period04* analysis are presented in Table 4 based on the amplitude variations as shown in Fig. 2. As described in Böhm et al. 2004, the uncertainty in the extracted frequency value can be estimated in different ways. The most conservative approach has been proposed by (Ripepi et al. 2003) who suggest to estimate the error by measuring the FWHM of the main lobe of the spectral window function, corresponding here to 0.31 d^{-1} , while (Kurtz & Müller 1999) use as an estimator the time basis ΔT of the observing run, yielding for the SAAO 1999 run a much smaller error estimate of $1/(4\Delta T) = 0.04\text{ d}^{-1}$. Breger et al. (1993) studied empirically the possibility of a peak in the periodogram being a true signal of pulsations with respect to the noise level; this work was refined later by Kuschnig et al. (1997): the significance of a peak in the amplitude periodogram exceeding 4.0 times the mean noise amplitude level after prewhitening of all local frequencies has a 99.9% probability to be due to stellar pulsations (99.0% for a ratio of 3.6, 90.0% for a ratio of 3.2). Fig. 3 shows the amplitude power spectrum including all strong peaks around 29 - 36 d^{-1} , the noise levels having been determined after prewhitening of the 9 first frequencies, while Fig. 4 shows the fact that even F_9 has a signal to noise level exceeding 4.0. We arbitrarily decided to stop the iterative procedure for amplitude values below 1%. The verification of the results with *Sigspec* revealed exactly the same frequencies and amplitudes, all detected frequencies F_1 to F_{10} having a significance level between 66.5 and 6.3, respectively. No combined frequency is present in the power spectrum, following the analysis with the *Combine* program by Reegen (2007). We don't attribute much importance to the frequencies below approximately 5 d^{-1} , since differential calibration issues from one night to the other might persist, i.e. this excludes F_4 , F_7 , F_8 and F_{10} . By applying the more conservative error estimate by (Ripepi et al. 2003), all remaining frequencies ("F") could be identified with the frequencies ("f") determined by radial velocity studies on the same data set in Böhm et al. (2004), F_3 being slightly outside the error bar, and the 1.0 d^{-1} difference between F_9 and f_3 indicates that we are most likely in presence of an alias of the same frequency. It can be noticed, that the order of the first two dominant frequencies is inverted depending if radial velocity or central depth variations are analysed.

4.2. Mode identification with the Fourier 2D method

A direct method of analysing the non-radial pulsation modes present in the LSD-spectra time series consists in applying the Fourier 2D method on line-profile variations (Kennelly et al. 1993; Kennelly 1994; Kennelly et al. 1996). This technique analyses the complex pattern present in the line profiles by computing a 2-dimensional Fourier transform in both time and Doppler space. To do this, an interpolation of each profile on a

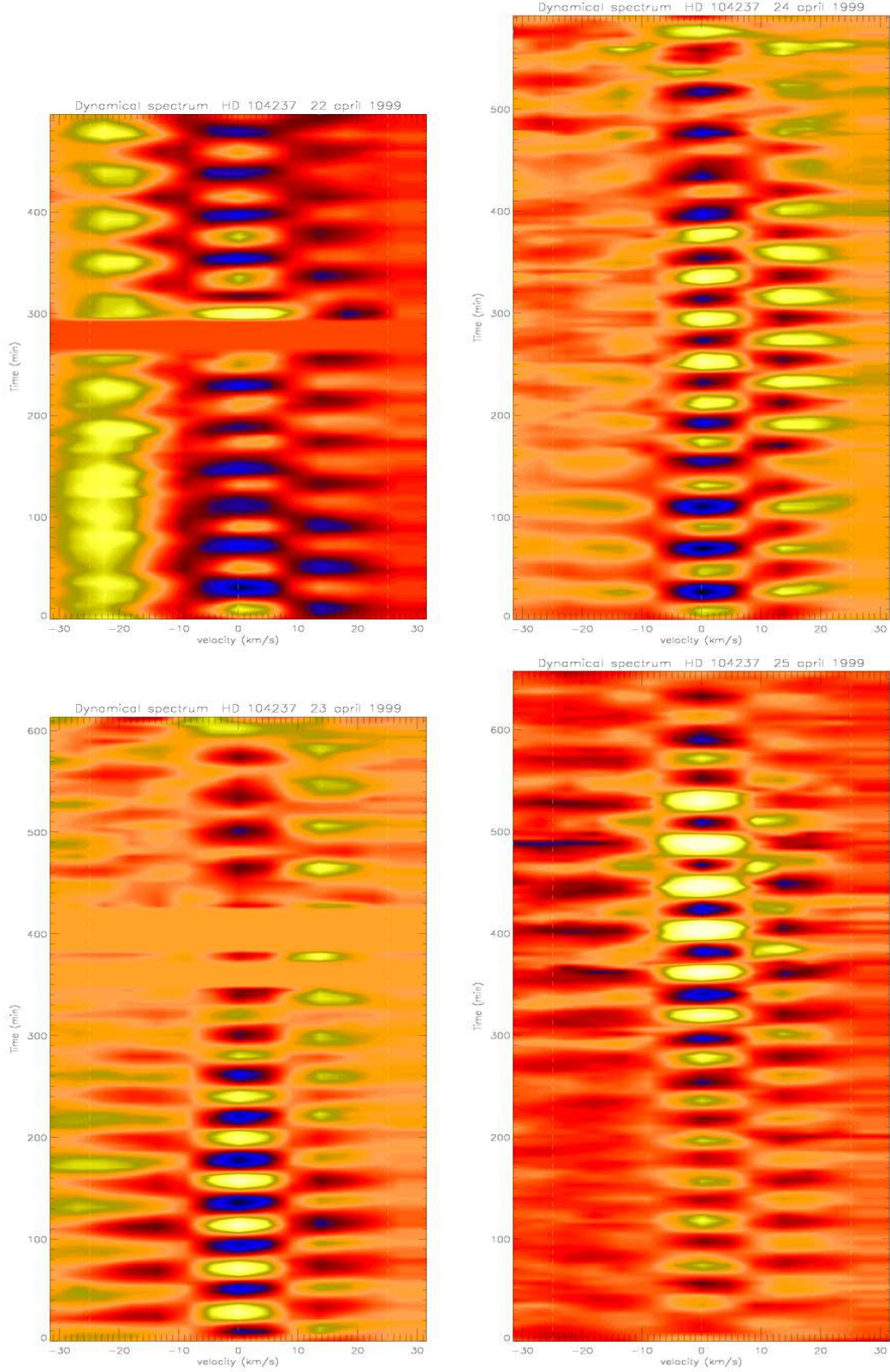


Fig. 1. Line profile variations due to the non-radial pulsations of HD 104237. The deviations from the mean intensity are displayed for four different nights (*top left*: April 22nd 1999, *bottom left*: 23rd 1999, *top right*: April 24th, *bottom right*: 25th 1999).

grid representing stellar longitudes is performed, transforming velocities across the line profile into longitudes on the stellar equator using the relation $\Delta v = v \sin i \sin \phi$. Δv is here the velocity position within the LSD profile with respect to the rest wavelength of the star and ϕ is the stellar longitude angle of the star in

spherical coordinates. In the resulting two-dimensional Fourier spectrum, the temporal frequencies are related here mainly to the frequencies of oscillation, while the apparent azimuthal order \hat{m} is related to the structure of the modes present at the stellar surface, without being identical to the usual azimuthal order m .

Table 4. Frequencies determined with *Period04*. The different columns are: (1) number, (2) frequency in d^{-1} and (3) in μHz . (4) Amplitude in (F/F_c) (flux variation with respect to the average profile), (5) identification with frequencies as of Böhm et al. (2004), and absolute shift in d^{-1} .

#	F_{P04} (d^{-1})	F_{P04} (μHz)	A_{P04} (F/F_c)	f_{B04} ($ \delta f $)
F_1	35.60	412.04	0.0089	f_2 (0.01)
F_2	33.74	390.51	0.0033	f_1 (0.12)
F_3	32.25	373.26	0.0030	f_6 (0.36)
F_4	4.47	51.74	0.0024	
F_5	31.08	359.72	0.0028	f_4 (0.12)
F_6	34.00	393.52	0.0019	f_5 (0.14)
F_7	1.94	22.45	0.0018	
F_8	2.72	31.48	0.0014	
F_9	29.48	341.20	0.0011	f_3 (1.0)
F_{10}	5.17	59.84	0.0010	

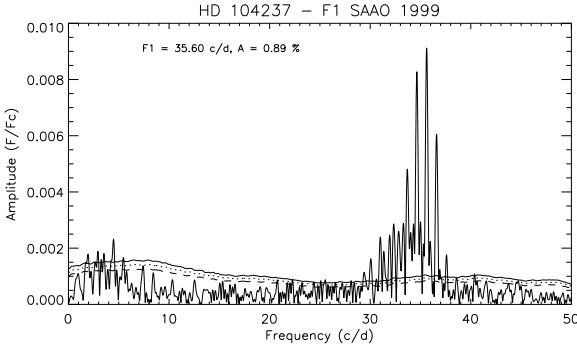


Fig. 3. Periodogram of the line center variation as shown in Fig. 2, without prewhitening. The large bulk of frequencies around 29 - 36 d^{-1} can be seen, as well as the 3.2, 3.6 and 4.0 mean-amplitude level of the noise determined by prewhitening F_1 to F_9 .

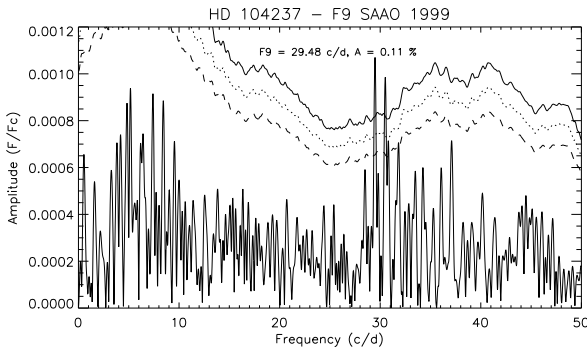


Fig. 4. Same figure as Fig. 3, but prewhitened by F_1 to F_8 . Only F_9 is present, well above the 99.9% confidence level.

The original work by Kennelly (1994) showed in fact that apparent $|m|$ scales as $\ell + 2$ for values close to zero, as $\ell + 1$ for values lower than 10 and as ℓ for values above 10. We performed this F2D computation on the night of April 22nd to 25th 1999. A weighted combination of the nightly F2D spectra can be seen in Fig. 5 (see Böhm et al. 2009 for details of the method) and

our results confirm the presence of low-degree non-radial pulsations: a peak at the dominant frequency F_1 is clearly seen with an apparent \hat{m} comprised between 2 and 4 indicating a degree ℓ comprised between 0 and 2. Moreover, as can be seen e.g. in Tab. 2.3 of Kennelly (1994) (or in simulation with available online-NRP simulators), the symmetric pattern of the dynamical residual profile as seen in Fig. 1 indicates for F_1 an azimuthal order $m = \pm 1$, implying a most likely ℓ value of 1 or 2.

The frequency peak in Fig. 5 between 3 and 5 d^{-1} is again not taken into account, since nightly calibration shifts can easily introduce such variations.

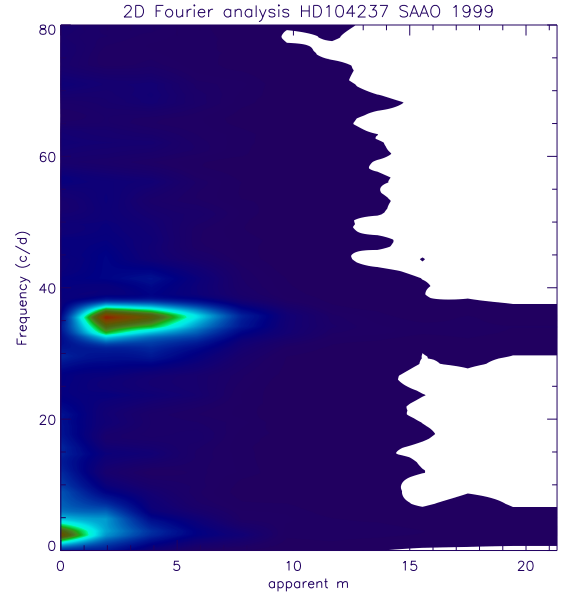


Fig. 5. Combined F2D analysis of HD 104237 for the nights of Apr. 22nd to 25th 1999.

A complementary analysis on the whole data set using the FAMIAS code (Zima et al. 2006; Zima 2008) is planned, but the highly asymmetric mean photospheric profile seen in HD 104237 adds complexity in the data analysis and cannot in the actual state of the code be taken into account.

5. Optimized spectral continuum determination

In addition to the best available mode identification, a future modeling of the stellar oscillations of HD 104237 requires the precise redetermination of its fundamental stellar parameters. Since we decided to carry out this analysis from reliably measured equivalent width of selected absorption lines (see Sect. 6), a perfect continuum normalization revealed to be essential, particularly in order to significantly increase the SNR by summing all the spectra of the night. An automatic code was therefore developed, the case of HD 104237 being rather complicated due to its spectroscopic binarity: the pollution of the primary (P) spectrum by the secondary (S), but also the presence of emission components and variability observed in numerous absorption lines require particular attention in the normalization procedure. The data set obtained at SAAO in 2000 (see Böhm et al. 2004) contained one night of observations very close to the periastron of the binary (12th of April). We decided therefore to concentrate on the data of this particular night in which both spectra are well separated in velocity, making easier to distin-

guish P from S. As we worked on echelle spectra, we carried out an individual normalization of each order, performed in 4 mainly automated main steps.

As a first step, we created a comb including effective continuum locations and eliminating unsuited others areas. To do so, we extracted 2 lists of absorption lines ($T_{\text{eff}}(\text{P}) = 8500 \text{ K}$ and $T_{\text{eff}}(\text{S}) = 4750 \text{ K}$, $\log g = 4.0$, $v_{\text{micro}} = 2 \text{ km s}^{-1}$ and solar abundances) from the Vienna Atomic Line Database (VALD; Piskunov et al. 1995; Ryabchikova et al. 1997; Kupka et al. 1999, 2000) on which we applied:

- i) a selective criterion on the maximum depth accepted for spectral lines to be considered as continuum ($\leq 1\%$ of the continuum), taking into account the relative luminosities of both components as a function of wavelengths, assuming two blackbodies with temperatures equal to 8500 K and 4750 K,
- ii) a criterion on the atypically large profile width of $\pm 2.5 v \sin i$ excluding areas with spectral lines,
- iii) the elimination of specific areas with emission, variable, telluric and the broad Balmer lines (the latter extending over several spectral orders and therefore not reliably to be normalized),
- iv) a shift of P and S wavelength grids by respective orbital velocities at the given observation time (all orbital parameters of the spectroscopic binary have been determined in Böhm et al. 2004).

After multiplication of the resulting comb with the observed spectrum, only wavelengths ranges corresponding to the remaining continuum areas were kept, all other areas were rejected. The next step consisted in fitting a polynomial of degree 4 through the remaining points in each order and a division of each order of the observed spectrum by this optimized polynomial. Finally, in a last step the software proceeds to a weighted concatenation of the normalized orders, the overlap between orders i and $i+1$ were taken into account through the following equation :

$$F_{\text{overlap}}(\lambda) = \frac{F_i(\lambda) \times \text{SNR}_i^2(\lambda) + F_{i+1}(\lambda) \times \text{SNR}_{i+1}^2(\lambda)}{\text{SNR}_i^2(\lambda) + \text{SNR}_{i+1}^2(\lambda)} \quad (1)$$

where $F_{\text{overlap}}(\lambda)$ is the total flux resulting from the addition of two overlapped parts of consecutive orders with normalized flux $F(\lambda)$, weighted by their corresponding local $\text{SNR}(\lambda)$, resulting from a polynomial fit of the respective SNR curve within the overlap, the local SNR being part of the reduced spectra files.

Since Balmer line profiles span several orders, they were not taken into account in this normalization process, i.e. area from 4816 to 4929 Å and from 6475 to 6645 Å remained unnormalized. During periastron both binary components show significant radial velocity shifts within one night. In order to sum up the large number of individual spectra during that night, we decided to center each individual spectrum to the rest wavelength of the primary component. Summation was thereafter done in the following way:

$$F_{\text{tot}}(\lambda) = \frac{\sum_{j=1}^n F_j(\lambda) \times \text{SNR}_j^2}{\sum_{j=1}^n \text{SNR}_j^2} \quad (2)$$

where $F_{\text{tot}}(\lambda)$ is, at each wavelength, the summed normalized spectrum, n is the number of spectra of the night, $F(\lambda)$ the individual flux, SNR is the mean SNR of each spectrum. After summation, the gain in SNR of our spectrum was of ≈ 6 since the SNR per resolved element at 550 nm increased from 64 to 372 (from 45 to 263 per pixel; see Fig. 6).

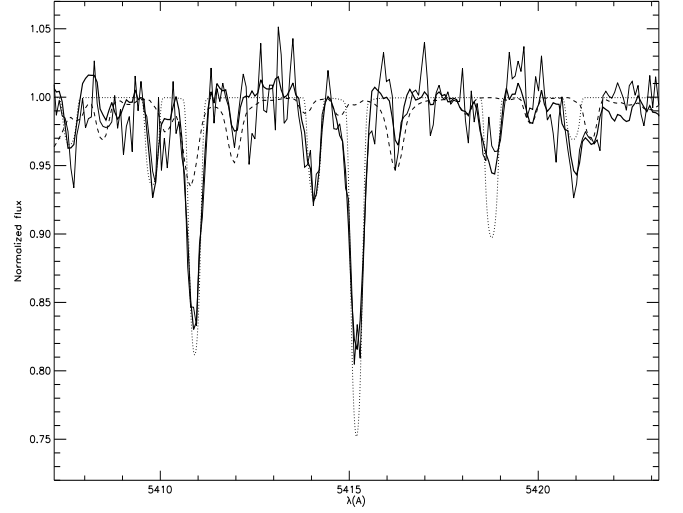


Fig. 6. Individual (thin line) and summed (thick line) normalized spectrum of the periastron night around one of the selected lines for our study (Fe I 5415.1920 Å). Synthetic spectra with $T_{\text{eff}} = 8500 \text{ K}$ (dotted line) and $T_{\text{eff}} = 4750 \text{ K}$ (dashed line) have been overplotted ($\log g = 4.0$, $v_{\text{micro}} = 2 \text{ km s}^{-1}$ solar abundances for both spectra), showing the location of the individual lines. The secondary spectrum has been corrected by the local luminosity ratio. The figure shows that the line selection process described in Sect. 6 works well. However, it can be noticed that either fundamental parameters and/or local luminosity ratios are not yet perfectly tuned at this stage.

6. Fundamental parameters determination

An accurate and reliable knowledge of stellar fundamental parameters, mainly effective temperature T_{eff} , surface gravity $\log g$ and chemical abundances $\log A$ (defined as follows: $\log A_E = \log \left(\frac{N_E}{N_H} \right)$ for an element E) is crucial to constrain the stellar atmosphere model, which is the basic ingredient of a forthcoming asteroseismic modeling. As shown in Sect. 2, for HD 104237 large discrepancies persist between parameters announced in the literature. A precise redetermination of its fundamental parameters is therefore crucial.

6.1. Method

Since T_{eff} , $\log g$, chemical abundances ($\log A$) and microturbulent velocity v_{micro} are interdependent and affect simultaneously the depth, width and shape of spectral absorption lines, they have therefore to be determined simultaneously. Numerous methods exist for such an analysis, but very few of them are suitable in the particular case of HD 104237. Due to the non standard shape of H A e Be spectral energy distributions (IR excesses, UV depletion), classical photometric determination of T_{eff} have to be considered with caution. Another frequently used method, the stellar parameter determination using Balmer lines have to be excluded because of core emission in the line and/or P Cygni profiles, but also on a technical side due to normalization issues in case of high dispersion echelle spectra. Techniques based on lines ratio for determining T_{eff} (see e.g. Sousa et al. 2010) require non polluted lines and were rejected because of strict selection criteria (see Subsect. 6.1.3), which excluded all workable lines in our case.

Table 5. Characteristics of absorption lines selected for fundamental parameters determination. Column are: (1) central wavelength, (2) ion, (3) excitation potential (eV), (4) log of statistical weight \times oscillator strength of the line transition, (5) local mean Signal to Noise, (6) observed equivalent width, (7) absolute and (8) relative uncertainty on the equivalent width.

λ_c (Å)	el.+ion.	χ_{eV}	$\log gf$	SNR	EW_{obs} (mÅ)	$\sigma_{\text{abs}}(EW_{\text{obs}})$ (mÅ)	$\sigma_{\text{rel}}(EW_{\text{obs}})$ (%)
4485.675	Fe I	3.686	-1.020	217	16.1	2.6	15.9
4602.941	Fe I	1.485	-2.209	245	39.3	4.0	10.1
5049.819	Fe I	2.279	-1.355	268	51.9	3.9	7.6
5132.669	Fe II	2.807	-4.094	275	28.0	4.0	14.5
5393.167	Fe I	3.241	-0.715	289	46.7	3.1	6.6
5415.192	Fe I	4.386	0.642	285	97.9	4.4	4.5
5434.523	Fe I	1.011	-2.122	273	51.9	3.3	6.3
5576.089	Fe I	3.430	-1.000	272	35.2	3.5	9.8
6084.111	Fe II	3.199	-3.881	245	18.2	4.0	21.8
6400.000	Fe I	3.602	-0.290	238	51.3	4.7	9.2

After consideration, we favoured an equivalent width (EW) analysis with respect to a direct spectrum fitting method, because of the existence of additional broadening agents and strong asymmetries in the line profiles, whose origin is unknown and which are therefore difficult to reproduce, and of numerous activity features in the whole spectrum that complicate direct line profile fitting. Our method consist in a comparison of EW of a set of selected lines, between the observed combined spectrum of the periastron night of HD 104237 and a fine grid of synthetic spectra in the 3 fundamental parameter dimensions, namely T_{eff} , $\log g$ and chemical abundance of a given chemical element (required to work out reliable values of T_{eff} and $\log g$). With more than 2000 spectral lines featured in a 8500 K synthetic spectra, Fe turned out to be the most suitable chemical element to establish our EW analysis. The high activity level of this HAe star (emission, variability, line asymmetry) and its binarity make a reliable determination of fundamental parameters in this case very challenging.

6.1.1. Correction of the secondary spectral contribution

Since our main goal was to determine the fundamental parameters of the primary component, we had to correct for the polluting spectroscopic contribution of the secondary component, HD 104237b. Indeed, although the secondary is significantly fainter than the primary component, it is also much cooler and does exhibit strong metallic absorption lines, leading to systematic contamination of primary lines and even lowering in some parts of the spectrum the continuum level. To free the observed spectrum from this effect, a synthetic spectrum corresponding to the secondary component was subtracted from the observed spectrum. In order to minimise additional errors from an incorrect model of secondary, we used stellar parameters determined by Böhm et al. (2004) based on cinematics of the binary movement, adopting solar chemical abundances, a $\log g$ value of 4.0 and a v_{micro} of 2 km s⁻¹: several synthetic spectra, with $T_{\text{eff}}(S)$ comprised between 4250 K and 5250 K (by step of 250 K) were therefore tested. Since the observed normalized spectra had been centered on the rest wavelength of the primary component, secondary synthetic spectra were shifted by the respective orbital velocity displacement. We called $\alpha(\lambda)$ a monochromatic luminosity ratio with $\alpha(\lambda) = B_P(\lambda)/B_S(\lambda)$, where $B_P(\lambda)$ and $B_S(\lambda)$ are respectively the Planck laws of the primary and the secondary. The most likely secondary model was determined by computing and minimizing a χ^2 quantity between the observed spectrum and the expected secondary contribution, yielding a T_{eff} value of 4500 K for the secondary. A spectrum corresponding to this tem-

perature ($F_S(\lambda)$ flux) was therefore subtracted from the observed spectra ($F_{\text{obs}}(\lambda)$ flux), with a contribution based on the equation:

$$F_{\text{obs}}(\lambda) = \frac{F_P(\lambda) + F_S(\lambda)/\alpha(\lambda)}{1 + 1/\alpha(\lambda)} \quad (3)$$

in order to obtain a primary spectrum ($F_P(\lambda)$ flux) cleaned up from the secondary contribution. Obviously, systematic uncertainties of the monochromatic luminosity ratio and the intrinsic stellar parameter selection of the secondary do persist and are difficult to fully be taken into account.

6.1.2. Construction of a 3D-grid of synthetic spectra

In order to precisely redetermine the fundamental parameters of our star we needed to compare the observed high SNR spectrum to synthetic spectra. Therefore, we constructed a 3-dimensional grid (T_{eff} , $\log g$, $\log A_{\text{Fe}}$) of synthetic spectra based on line catalogs provided by the VALD database (see Sect.5) as input of the SYNTH3 spectrum synthesis code (Kochukhov 2007), each spectrum covering a wavelength range from 4400 Å to 7000 Å. The SYNTH3 code assumes Local Thermodynamic Equilibrium (LTE) and a plane-parallel hydrostatic stellar model atmosphere. For early type stars input models are provided by the well known Kurucz program suite. We selected solar abundance atmosphere models from the grid, after having checked that the effect of an input model containing slightly different than solar metallicities is of second order on the calculated synthetic spectrum.

As a starting point, we adopted parameters derived by previous authors to define the boundaries of the grid: $7500 \text{ K} \leq T_{\text{eff}} \leq 9500 \text{ K}$ (by steps of 250 K) and $3.5 \leq \log g \leq 4.5$ (by steps of 0.5). Since it is not uncommon to find HAeBe stars exhibiting in their spectra simultaneously the presence of some elements in suprasolar abundance, whereas other ones are sub-solar (see e.g. Acke & Waelkens 2004), without particular trend in terms of global metallicity, we decided to modify in this study only the Fe abundance in our VALD requests. It should be noticed at this stage, that studying the iron abundancy was a necessary by-product in order to constrain effective temperature, as we will see subsequently. $\log A_{\text{Fe}}$ values comprised between -4.84 and -4.00 seemed to be reasonable, i.e. $[\text{Fe}/\text{H}]$ values comprised between -0.3 and +0.54 with respect to the solar Fe abundance given in VALD, which adopted $\log A_{\text{Fe}\odot} = -4.54$. As a reminder, $[\text{Fe}/\text{H}] = \log\left(\frac{N_{\text{Fe}}}{N_{\text{H}}}\right)_{\star} - \log\left(\frac{N_{\text{Fe}}}{N_{\text{H}}}\right)_{\odot}$. Typical values of v_{micro} found in the literature were of 2-3 km s⁻¹ (see e.g. Acke & Waelkens 2004; Guimarães et al. 2006; Catala et al. 2007), we therefore fixed a value of 2 km s⁻¹ for the microturbulent velocity HD 104237. A wavelength by wavelength quadratic

interpolation was subsequently done between synthetic spectra in order to obtain a finer spectral grid with a 25 K step in T_{eff} , a 0.1 step in $\log g$ and a 0.01 step in $\log A_{\text{Fe}}$.

6.1.3. Photospheric line selection

Photospheric iron absorption lines used in our study were selected using the following criteria:

- exist for every (T_{eff} , $\log g$, $\log A_{\text{Fe}}$) triplet in order to be intercomparable;
- exclude blends with lines from other chemical elements (than Fe), i.e. within a range of $\pm 2.3 \nu \sin i/c$ from the central wavelength (the extraction width having been adopted after visually inspecting the spectra and taking into account the broad wings of the photospheric lines of our star);
- avoid pollution by lines from the secondary spectrum, even if a best-fit secondary spectrum had been removed, in order to minimise the impact of the potential error on $T_{\text{eff}}(S)$. To do so, secondary lines with a relative contribution deeper than 10% of the central depth led to a rejection of the primary spectrum line.
- show no or little variability in time (especially over short periods of time);
- do not exhibit at any time an emission or other than normal (for HD 104237) asymmetry;
- be strong enough with respect to local noise, in order to minimize relative uncertainties on EW and to be able to neglect residual contribution from very faint lines of primary and secondary spectra (VALD requests require a depth threshold and provide catalog of lines deeper than this threshold value), but not too strong to avoid saturation effects. As a result, we kept weak and moderately strong lines ($15 \text{ m}\text{\AA} \leq \text{EW}_{\text{obs}} \leq 100 \text{ m}\text{\AA}$);
- show exploitable nearby continuum, e.g. with no emission component in their immediate vicinity (after automatic selection, a individual visual check line by line was done);
- cover a variety of excitation potentials, ionization stages and wavelengths;
- having ascertained atomic parameters, in particular $\log gf$ values (comparison with Fuhr & Wiese 2006 and Meléndez & Barbuy 2009).

This rigorous selection resulted in a set of only 10 spectral lines (8 Fe I lines and 2 Fe II lines) which are listed in Table 5.

6.1.4. EW measurements

EW measurements of our selected lines were carried out using a trapezoidal integration. For consistency, the identical extraction limits were used for the integration of a given line from both the observed spectrum and the synthetic spectra.

To extract errors on EW values, we assumed that they mainly came from local averaged photon noise and we neglected uncertainties in integration limits or arising from residual continuum normalization errors. Multiplying the local $\overline{\text{SNR}}$ value by the line integration width $\Delta \nu$ of each line, we then obtained an estimation of absolute uncertainty in EW, $\sigma_{\text{abs}}(\text{EW}_{\text{obs}})$, and its corresponding relative uncertainty $\sigma_{\text{rel}}(\text{EW}_{\text{obs}}) = \sigma_{\text{abs}}(\text{EW}_{\text{obs}})/\text{EW}_{\text{obs}}$ (see Table 5).

6.2. T_{eff} , $\log g$ and Fe abundance determination

In order to determine T_{eff} , $\log g$ and $\log A_{\text{Fe}}$ of HD 104237, it was necessary to compute the degree of similarity between our observed spectrum and all the synthetic spectra of our 3D-grid by means of the 10 previously measured EW; a direct synthetic spectrum fitting technique could not be applied due to highly atypical photospheric line profiles (asymmetry, broad wings).

A maximum likelihood estimation was therefore done by minimizing the following reduced merit function S_{red} :

$$S_{\text{red}} = \frac{1}{N-k} \sum_{j=1}^N \left(\frac{\text{EW}_{\text{obs},j} - \text{EW}_{\text{synth},j}(T_{\text{eff}}, \log g, \log A_{\text{Fe}})}{\sigma_j} \right)^2 \quad (4)$$

where $N-k$ is the number of degrees of freedom, N being the number of selected lines and k being the number of parameters to be determined (3 in our case). A good introduction to this statistical approach can be found in Press et al. (1992). EW_{obs} and EW_{synth} are respectively the EW of the observed spectrum and the EW of a synthetic spectrum, S_{red} being computed for each synthetic spectrum of our 3D-grid. Lastly, σ corresponds to the uncertainty on both EW_{obs} and EW_{synth} such that $\sigma^2 = \sigma_{\text{obs}}^2 + \sigma_{\text{synth}}^2$. Because of the optimal normalization and the absence of noise in synthetic spectra, σ_{synth} was neglected and we assumed that $\sigma = \sigma_{\text{obs}}$, σ_{obs} being described in Sect. 6.1.4 and in Table 5 as $\sigma_{\text{abs}}(\text{EW}_{\text{obs}})$. The error bars on the parameters of the synthetic spectrum yielding the lowest value of S_{red} were then investigated by means of statistical tools. The merit function S_{red} follows a χ^2 distribution with $\nu = N-k$ degrees of freedom if: i) we consider that the best model supplied by the minimum merit function is the right physical model representing the star and therefore that the corresponding stellar parameters are the true parameters of the star, ii) we assume that the perturbations on $(\text{EW}_{\text{obs}} - \text{EW}_{\text{synth}})$ are independent and additive standard normal random variables. Since the σ_{obs} values are estimated from the local SNR around the selected lines and since the noise is poissonian and tends to a gaussian distribution in case of a great number of photons, which is the case here, the gaussian assumption is valid in this study. In this situation, the error bar corresponding to a chosen confidence interval x can be provided by the cumulative distribution function of the χ^2 distribution with ν degrees of freedom defined as:

$$D_{\nu}(x) = \int_0^x \frac{t^{\frac{\nu}{2}-1} e^{-\frac{t}{2}}}{\Gamma(\frac{\nu}{2}) 2^{\frac{\nu}{2}}} dt = \frac{\gamma(\frac{\nu}{2}, \frac{x}{2})}{\Gamma(\frac{\nu}{2})} \quad (5)$$

where Γ and γ denote the Gamma and lower incomplete Gamma function, respectively. $D_{\nu}(x)$ is equal to the probability $\mathbb{P}(S \leq x)$ of the merit function $S = S_{\text{red}} \times (N-k)$ to be within the confidence interval x . By misuse of language, such confidence intervals on the S value are usually considered to be equivalent to confidence intervals on the resulting parameters. For the needs of our study, we did the same assumption. We were therefore searching for the interval ΔS such that $S_{\text{min}} + \Delta S \leq x$, which was equivalent to search for $\Delta S_{\text{red}} = \Delta S/(N-k)$ such that $S_{\text{red},\text{min}} + \Delta S_{\text{red}} \leq x/(N-k)$. With $\nu = 10 - 3 = 7$ degrees of freedom we deduced that parameters of synthetic spectra included within an interval ΔS_{red} of 1.17, 2.04 and 3.12 from the minimum $S_{\text{red},\text{min}}$ value were respectively 68.3%, 95.4% and 99.7% reliable.

A preliminary computation of S_{red} within the whole 3D-grid of synthetic spectra, without any constraint, yielded a T_{eff} value of 8775 K, a $\log g$ value of 4.2 and a $\log A_{\text{Fe}}$ value of -4.25 , i.e. $[\text{Fe}/\text{H}] = +0.29$ (the solar abundance being $\log(\frac{N_{\text{Fe}}}{N_{\text{H}}})_{\odot} = -4.54$). The corresponding error bars were

estimated using the method described above. For a confidence level of 68.3%, we found the following uncertainties: 525 K on T_{eff} , 0.7 on $\log g$ and 0.35 on $\log A_{\text{Fe}}$. For a confidence level of 95.4%, we determined the uncertainties of 700 K on T_{eff} and 0.48 on $\log A_{\text{Fe}}$, the small sensitivity to $\log g$ does not allow the determination of the 95.4% confidence level for $\log g$ within our parameter space. The results are shown in Fig. 7.

What we pointed out at this stage were the limits of this first statistical computation due to the very low number of drastically selected lines used in the merit function minimization, that led to a significant T_{eff} and $\log g$ degeneracy: numerous synthetic spectra yielded S_{red} values within the chosen confidence intervals, and a much larger number of selected lines would have been necessary to converge reliably towards the model best representing the observations with smaller error bars. This effect was also pointed out by the results of a jackknife resampling, which consisted in recomputing several times the merit function S_{red} , leaving out one after each other the equivalent width of one line. This statistical method revealed that the *best parameters* could change depending on the removed line within a ΔT_{eff} of $^{+150}_{-200}$ K, a $\Delta \log g$ of $^{+0.2}_{-0.3}$ and a $\Delta \log A_{\text{Fe}}$ of $^{+0.10}_{-0.09}$. This line-dependance of the result was attributed to the lack of selected lines too. To compensate for this lack, we confronted our preliminary result to the additional physical constraint brought by the excitation equilibrium: indeed, if T_{eff} is well determined, all spectral lines corresponding to a specified ion, and with a given excitation potential, should provide the same abundance determination. In a first step, for consistency, we only kept stellar model couples (T_{eff} , $\log g$) for which the equivalent width EW of all selected Fe I lines had an intersection with the curve of growth (EW_{synth} as a function of $\log A_{\text{Fe}}$) within the range of our parameter space. In a second step we calculated for each selected model linear regression lines through the 8 data points $\log A_{\text{Fe}} = f(\chi)$ (χ being the excitation potential, usually expressed in eV) and kept only the stellar models yielding a close to zero slope regression line (in fact we calculated a standard deviation of the distribution of all slopes, and kept models with slopes $0 \pm 1 \sigma$). Fig. 8 shows the fact that for each T_{eff} a small range of $\log g$ and $\log A_{\text{Fe}}$ couples agreed with the excitation equilibrium within the error bar.

Taking the excitation equilibrium into consideration, we excluded models not respecting it and searched again for the minimum value of S_{red} . We obtained: $T_{\text{eff}} = 8550$ K, $\log g = 3.9$ and $\log A_{\text{Fe}} = -4.38$. To determine the error bar on these parameters, we adopted the same approach as described previously in this section. It should be noted that $\log g$ is the less accurately determined stellar parameter because of the fainter sensibility of the selected lines to this parameter. The results can be seen in Fig. 9 and are summarized in Table 6. The shape of the 2D-repartition of the S_{red} values showed in Fig. 9 can be understood from Fig. 7 and Fig. 8.

Table 6. Fundamental parameters of HD 104237 determined in this study.

stellar param.	best model param. values	68.3% conf. int.	95.4% conf. int.
T_{eff} (K)	8550	± 150	± 225
$\log g$	3.9	± 0.3	± 0.4
$\log A_{\text{Fe}}$ ()	-4.38	± 0.19	± 0.26
[Fe/H] ()	+0.16	± 0.19	± 0.26

In order to check the validity of our result, we plotted the abundances determined from the 8 Fe I selected lines as a function of their excitation potential in the case of the model minimizing S_{red} without any additional constraint and of the model minimizing S_{red} with excitation equilibrium constraint. The result can be seen in Fig. 10. The linear regression across the points of the model with $T_{\text{eff}} = 8775$ K shows a negative slope, whereas the one across the points of the model with $T_{\text{eff}} = 8550$ K shows a flat regression line, which confirmed this model as the best solution.

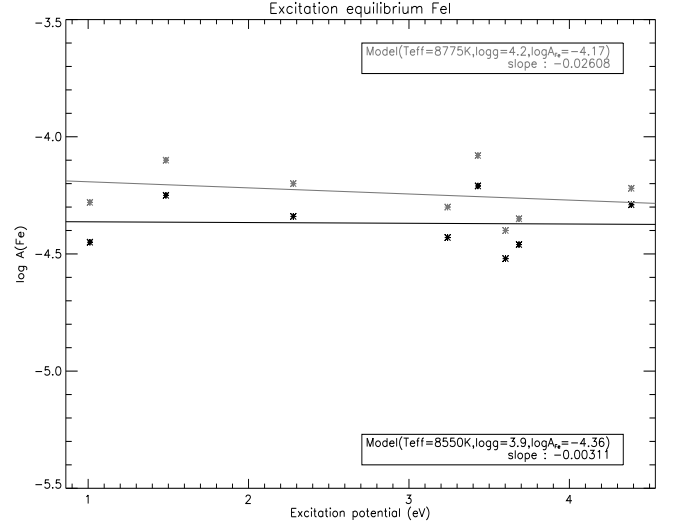


Fig. 10. Excitation equilibrium of Fe I. In black: the model minimizing S_{red} with excitation equilibrium constraint. In grey: the model minimizing S_{red} without any additional constraint.

Another successful verification of the reliability of our results consisted in verifying the iron ionization equilibrium, i.e. that an optimal model must give the same abundances derived from Fe I and Fe II.

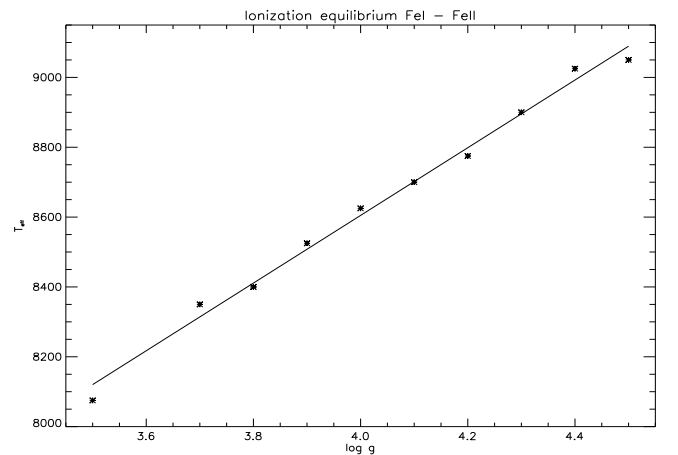


Fig. 11. T_{eff} and $\log g$ pairs respecting the ionization equilibrium between Fe I and Fe II lines in HD 104237. Stars: T_{eff} and $\log g$ values derived from the HD 104237 spectrum; the line shows a linear regression.

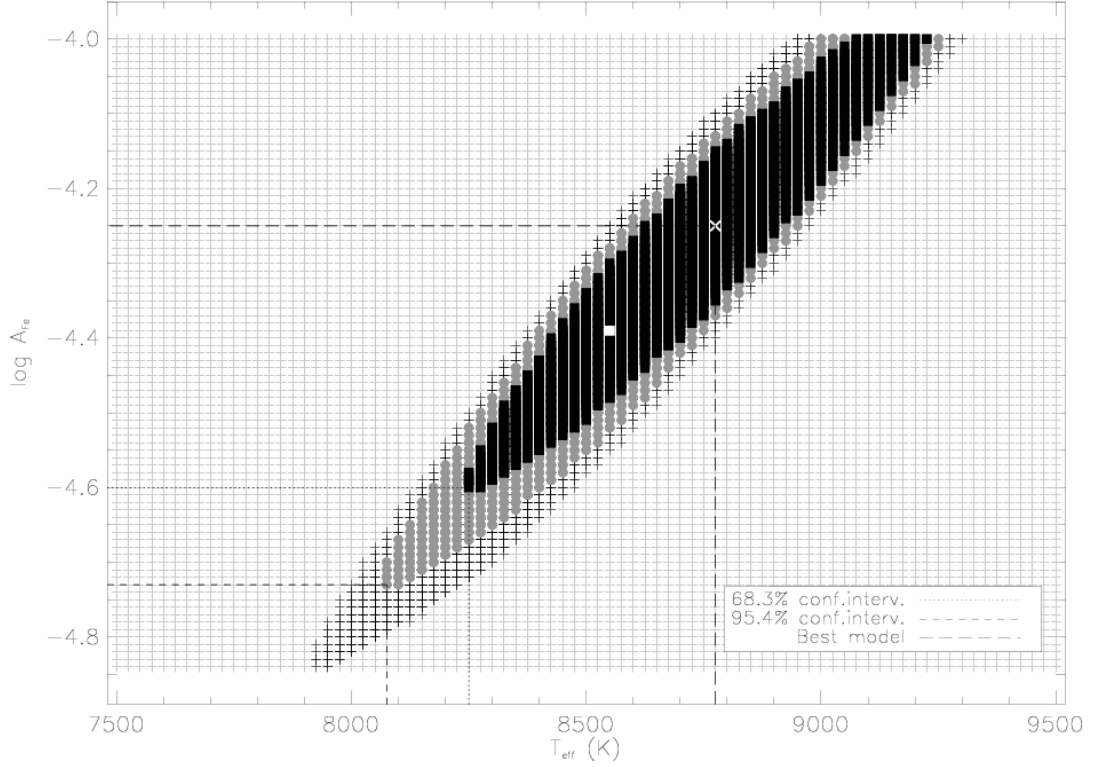


Fig. 7. 2D-repartition of the S_{red} values as a function of T_{eff} and $\log A_{\text{Fe}}$. This graph has been built by considering successively every value of $\log g$, from 3.5 to 4.5 by step of 0.1. The white X represents the best model, whose $T_{\text{eff}} = 8775$ K, $\log A_{\text{Fe}} = -4.25$ and $\log g = 4.2$. The boundary 68.3%, 95.4% and 99.7% confidence intervals are respectively marked by the dotted lines and the black filled squares, the dashed lines and the grey filled circles and the black crosses. The grey cross represent the T_{eff} and $\log A_{\text{Fe}}$ ranges investigated in the present study from error box found in the literature, keeping in mind that $\log g$ values range from 3.5 to 4.5. The white filled square locates the best model with the additional excitation equilibrium constraint described in the continuation of the Sect. 6.2.

7. Discussion and Conclusions

In this article we presented an in-depth analysis of the prototype Herbig Ae star HD 104237. The star has been previously identified as a PMS δ Scuti pulsator, and the comprehensive line profile analysis of the extended quasi-continuous high resolution spectroscopic time series obtained at SAAO from April 22nd - 26th 1999 has confirmed the main frequencies discovered by radial velocity analysis in Böhm et al. (2004). For the first time, the less than 1.5 % continuum level variations of the equivalent photospheric LSD profiles were studied and a direct confirmation of the presence of at least one non radial pulsations could be performed. Based on a Fourier 2D analysis we identified the dominant mode as an azimuthal order $m = \pm 1$, and a most likely ℓ value of 1 or 2. Since HD 104237 is a moderate rotator with $v \sin i$ of only 12 ± 2 km s⁻¹ it will be difficult getting access to additional mode identifications in the future, a potential approach would be to organize multi-site continuous observations with significantly higher resolution echelle spectrographs, ideally with $R \geq 70000$. On the mode identification aspect a modification of the FAMIAS code working with asymmetric photospheric profiles would be a great progress.

In order to prepare a forthcoming asteroseismic modeling of this particular star we needed to determine very precisely its fundamental stellar parameters. Since HD 104237 is a multiple system with a nearby spectroscopic binary companion, we decided to concentrate on the periastron night of 12th of April

2000, present in our data set of spectra acquired at SAAO (and described in Böhm et al. 2004). To combine all spectra of this particular night to one high SNR reference spectrum, we developed an optimized spectral continuum determination tool. As a result, the reference spectrum had a SNR value of close to 400 per resolved element at 550 nm.

The detailed study of the fundamental stellar parameters has provided values of $T_{\text{eff}} = 8550 \pm 150$ K, $\log g = 3.9 \pm 0.3$ and $\log A_{\text{Fe}} = 4.38 \pm 0.19$ (i.e. $[\text{Fe}/\text{H}] = +0.16 \pm 0.19$), the error bars corresponding to the 68.3% confidence interval. A particular effort was put on the statistically correct determination of the associated error bars. In a review of T_{eff} and $\log g$ determination methods, Smalley (2005) mentioned optimal error bars to be of ± 100 K for T_{eff} , ± 0.2 for $\log g$ and of the order of 0.05 to 0.1 in abundance. Due the high level of activity of HAeBe stars, and in the case our target star the spectroscopic binarity, it is very difficult to obtain a sufficiently large number of unpolluted, exploitable photospheric spectral lines of a given ion; the achievable uncertainties remain therefore rather large. In addition, a wrong estimate of the contribution of the secondary, both in spectral class and in luminosity, might lead to systematic errors which are very difficult to take into account. However, we estimate these errors to be of second order in our study.

The surface gravity being difficult to constrain in our spectroscopic approach, the associated luminosity ratio (based on the empirical mass-luminosity relation by Malkov 2007) was determined to $\log (L_{\star}/L_{\odot}) = 1.59 \pm 0.44$, a value centered on

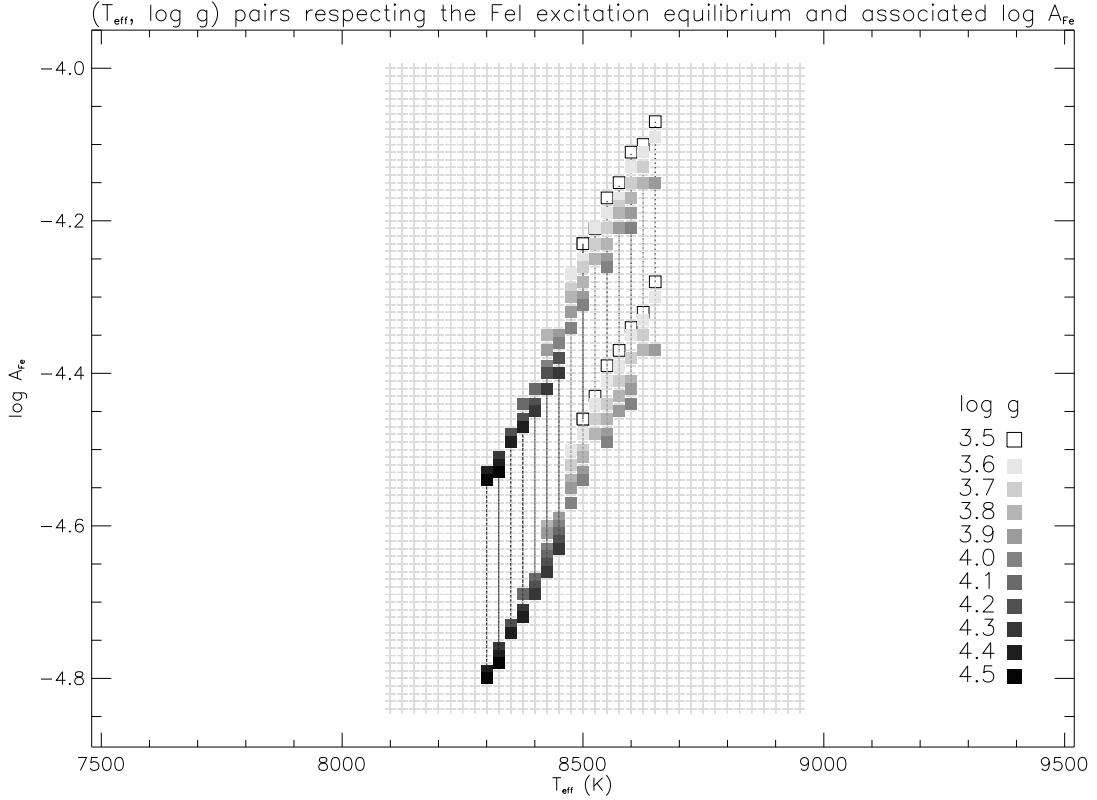


Fig. 8. (T_{eff} , $\log g$) pairs respecting the Fe I excitation equilibrium and associated $\log A_{\text{Fe}}$ ranges (dotted lines delimited by squares). Each color of square, from lightest grey to darkest grey, represents a value of $\log g$ from 3.5 to 4.5. Grey crosses represent the subspace of models for which there exists an intersection between the EW_{obs} line and the curve of growth for every one of the 8 selected Fe I lines.

the result by van den Ancker et al. (1998), whose authors determined $\log(L_{\star}/L_{\odot}) = 1.55^{+0.06}_{-0.05}$. On the contrary, our spectroscopic effective temperature determination is significantly improved with $T_{\text{eff}} = 8550 \pm 150$ K, again centered on the central value of van den Ancker et al. (1998), whose result was $T_{\text{eff}} = 8500 \pm 500$ K. Our independent spectroscopic approach therefore tends to confirm the previously photometrically determined values by van den Ancker et al. (1998). Combining the two results would yield the following most likely fundamental parameters: $\log(L_{\star}/L_{\odot}) = 1.55^{+0.06}_{-0.05}$, corresponding to $\log g = 3.93 \pm 0.09$, and $T_{\text{eff}} = 8550 \pm 150$ K. Fig. 12 shows well the intersection between our new results and previously determined parameters from van den Ancker et al. (1998). At this stage it is important to mention that error bars by van den Ancker et al. (1998) and Grady et al. (2004) might be largely underestimated.

Acke & Waelkens (2004) determined an iron abundance of Fe ($[\text{Fe}/\text{H}] = +0.09 \pm 0.19$). Our new result of the abundance, $[\text{Fe}/\text{H}] = +0.16 \pm 0.19$, confirms the conclusion that HD 104237 might be slightly overabundant. Vick et al. (2011) calculated recently self-consistent stellar evolution models in this mass range including atomic diffusion; they concluded that for mass loss ranges above $10^{-12} \text{ M}_{\odot} \text{ yr}^{-1}$ no surface abundance anomalies are expected. HD 104237 shows a very strong H_{α} line with a complex profile, which tends to indicate significantly higher mass loss rates, similar to other Herbig Ae stars showing typical mass loss rates of the order of $10^{-7} - 10^{-8} \text{ M}_{\odot} \text{ yr}^{-1}$ (see e.g. Bouret & Catala 1998). Taking these new simulations into account, we conclude on a close to solar iron abundance for HD 104237, which is clearly within the error bars of both studies.

We want to mention at this stage that several assumptions have been made in this study, on the modeling side (LTE, plane-parallel spectrum synthesis), on the contribution of the faint secondary (ratio of planck functions), on the threshold of line selection, but also the assumed photospheric line formation region of our lines of interest, amongst others. Despite the fact that these residual errors should be negligible with respect to our study, further improvements on line selection and analysis, such as a combined treatment of blended lines, will lead to more and more constrained fundamental parameters in the future.

A forthcoming article (Fumel et al. 2011) will describe the asteroseismic modeling of the primary component of HD 104237.

Acknowledgements. The authors want to thank N. Grevesse for interesting and fruitful discussions about stellar parameters determination and his critical advices about atomic parameters. Warm thanks also to H. Carfantan for precious discussions about the statistically meaningful use of the χ^2 quantity and his advices concerning error bar determination in multiple dimension parameter spaces. Many thanks also to F. Lignières, P. Petit and P. Fouqué for their important comments on the approach we adopted. We acknowledge the Vienna Atomic Line Data base we used for our research work. Our thoughts are going to P. Reegen for his important contribution to time series analysis.

References

- Acke, B. & Waelkens, C. 2004, *A&A*, 427, 1009
- Anders, E. & Grevesse, N. 1989, *Geochim. Cosmochim. Acta*, 53, 197
- Baines, D., Oudmaijer, R. D., Porter, J. M., & Pozzo, M. 2006, *MNRAS*, 367, 737
- Bertout, C., Basri, G., & Bouvier, J. 1988, *ApJ*, 330, 350
- Böhm, T. & Catala, C. 1995, *A&A*, 301, 155
- Böhm, T., Catala, C., Balona, L., & Carter, B. 2004, *A&A*, 427, 907

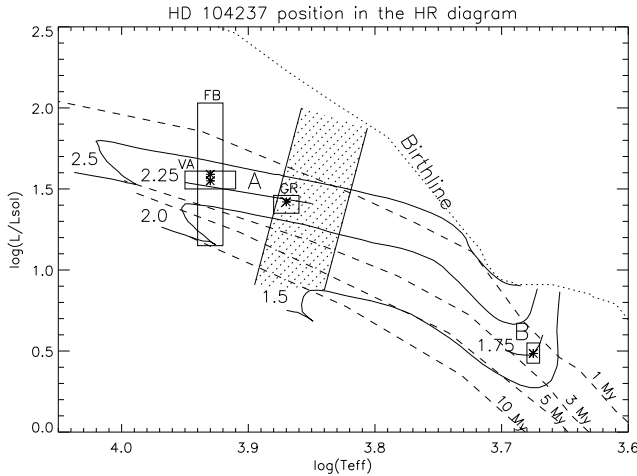


Fig. 12. New fundamental stellar parameters of the primary (A) component of HD 104237, located in the HR diagram from Böhm et al. (2004). The location of the secondary component HD 104237 b (B) is also indicated. The luminosity and effective temperature pairs reported in van den Ancker et al. (1998) (VA) and Grady et al. (2004) (GR) are shown in the diagram, including their *estimated* error bars, along with our new parameters (FB), associated with error bars corresponding to the 68.3% confidence interval. Evolutionary tracks (1.5, 2.0 and 2.5 M_{\odot}) and isochrones are by Palla & Stahler (2001). The Marconi & Palla (1998) instability strip is represented by the shaded area

Böhm, T., Catala, C., Donati, J.-F., et al. 1996, A&AS, 120, 431
 Böhm, T., Dupret, M. A., & Aynedjian, H. 2006, Mem. Soc. Astron. Italiana, 77, 362
 Böhm, T., Zima, W., Catala, C., et al. 2009, A&A, 497, 183
 Bouret, J.-C. & Catala, C. 1998, A&A, 340, 163
 Breger, M. 1972, ApJ, 171, 539
 Breger, M., Stich, J., Garrido, R., et al. 1993, A&A, 271, 482
 Brown, A., Djie, H. R. E. T. A., Blondel, P. F. C., et al. 1997, in Astronomical Society of the Pacific Conference Series, Vol. 121, IAU Colloq. 163: Accretion Phenomena and Related Outflows, ed. D. T. Wickramasinghe, G. V. Bicknell, & L. Ferrario, 448–+
 Catala, C. 1988, A&A, 193, 222
 Catala, C. 2003, Ap&SS, 284, 53
 Catala, C., Alecian, E., Donati, J.-F., et al. 2007, A&A, 462, 293
 Catala, C., Böhm, T., Donati, J.-F., & Semel, M. 1993, A&A, 278, 187
 Catala, C., Czarny, J., Felenbok, P., & Praderie, F. 1986a, A&A, 154, 103
 Catala, C., Donati, J. F., Böhm, T., et al. 1999, A&A, 345, 884
 Catala, C., Felenbok, P., Czarny, J., Talavera, A., & Boesgaard, A. M. 1986b, ApJ, 308, 791
 Catala, C. & Kunasz, P. B. 1987, A&A, 174, 158
 Catala, C. & Talavera, A. 1984, A&A, 140, 421
 Donati, J., Semel, M., Carter, B. D., Rees, D. E., & Collier Cameron, A. 1997, MNRAS, 291, 658
 Dupret, M.-A., Böhm, T., Goupil, M.-J., Catala, C., & Grigahcene, A. 2006, Communications in Asteroseismology, 147, 72
 Dupret, M.-A., Théado, S., Böhm, T., et al. 2007, Communications in Asteroseismology, 150, 59
 Feigelson, E. D., Lawson, W. A., & Garmire, G. P. 2003, ApJ, 599, 1207
 Fuhr, J. R. & Wiese, W. L. 2006, Journal of Physical and Chemical Reference Data, 35, 1669
 Fumel, A., Dupret, M.-A., & Böhm, T. 2011, A&A, in prep.
 Gilliland, R. L. 1986, ApJ, 300, 339
 Grady, C. A., Woodgate, B., Torres, C. A. O., et al. 2004, ApJ, 608, 809
 Guimarães, M. M., Alencar, S. H. P., Corradi, W. J. B., & Vieira, S. L. A. 2006, A&A, 457, 581
 Herbig, G. H. 1960, ApJS, 4, 337
 Hu, J. Y., Blondel, P. F. C., The, P. S., et al. 1991, A&A, 248, 150
 Hu, J. Y., The, P. S., & de Winter, D. 1989, A&A, 208, 213
 Iben, I. & Renzini, A. 1984, Phys. Rep., 105, 329
 Iben, Jr., I. 1965, ApJ, 141, 993
 Kennelly, E. J. 1994, PhD thesis, THE UNIVERSITY OF BRITISH

COLUMBIA (CANADA).

Kennelly, E. J., Walker, G. A. H., Catala, C., et al. 1996, A&A, 313, 571
 Kennelly, E. J., Walker, G. A. H., Matthews, J. M., & Merryfield, W. J. 1993, in Astronomical Society of the Pacific Conference Series, Vol. 42, GONG 1992. Seismic Investigation of the Sun and Stars, ed. T. M. Brown, 359–+
 Kochukhov, O. P. 2007, in Physics of Magnetic Stars, 109–118
 Kupka, F., Piskunov, N., Ryabchikova, T. A., Stempels, H. C., & Weiss, W. W. 1999, A&AS, 138, 119
 Kupka, F. G., Ryabchikova, T. A., Piskunov, N. E., Stempels, H. C., & Weiss, W. W. 2000, Baltic Astronomy, 9, 590
 Kurtz, D. W. & Marang, F. 1995, MNRAS, 276, 191
 Kurtz, D. W. & Müller, M. 1999, MNRAS, 310, 1071
 Kuschnig, R., Weiss, W. W., Gruber, R., Bely, P. Y., & Jenkner, H. 1997, A&A, 328, 544
 Lenz, P. & Breger, M. 2005, Communications in Asteroseismology, 146, 53
 Lignieres, F., Catala, C., & Manganey, A. 1996, A&A, 314, 465
 Luhman, K. L. 2004, ApJ, 616, 1033
 Lyo, A.-R., Lawson, W. A., & Bessell, M. S. 2008, MNRAS, 389, 1461
 Malkov, O. Y. 2007, MNRAS, 382, 1073
 Marconi, M. & Palla, F. 1998, ApJ, 507, L141
 Marconi, M. & Palla, F. 2004, in IAU Symposium, Vol. 224, The A-Star Puzzle, ed. J. Zverko, J. Ziznovsky, S. J. Adelman, & W. W. Weiss, 69–79
 Meus, G., Waters, L. B. F. M., Bouwman, J., et al. 2001, A&A, 365, 476
 Meléndez, J. & Barbuy, B. 2009, A&A, 497, 611
 Palla, F. & Stahler, S. W. 1990, ApJ, 360, L47
 Palla, F. & Stahler, S. W. 1993, ApJ, 418, 414
 Palla, F. & Stahler, S. W. 1999, ApJ, 525, 772
 Palla, F. & Stahler, S. W. 2001, ApJ, 553, 299
 Piskunov, N. E., Kupka, F., Ryabchikova, T. A., Weiss, W. W., & Jeffery, C. S. 1995, A&AS, 112, 525
 Praderie, F., Catala, C., Simon, T., & Boesgaard, A. M. 1986, ApJ, 303, 311
 Praderie, F., Felenbok, P., Czarny, J., Talavera, A., & Boesgaard, A. M. 1982, ApJ, 254, 658
 Press, W. H., Teukolsky, S. A., Vetterling, W. T., & Flannery, B. P. 1992, Numerical recipes in FORTRAN. The art of scientific computing, ed. Press, W. H., Teukolsky, S. A., Vetterling, W. T., & Flannery, B. P.
 Reegen, P. 2007, A&A, 467, 1353
 Ripepi, V., Marconi, M., Bernabei, S., et al. 2003, A&A, 408, 1047
 Ryabchikova, T. A., Piskunov, N. E., Kupka, F., & Weiss, W. W. 1997, Baltic Astronomy, 6, 244
 Schmidt-Kaler, T. 1982, in Landolt-Börnstein Catalogue VI/2b
 Siess, L., Dufour, E., & Forestini, M. 2000, A&A, 358, 593
 Smalley, B. 2005, Memorie della Societa Astronomica Italiana Supplementi, 8, 130
 Sneden, C. A. 1973, PhD thesis, THE UNIVERSITY OF TEXAS AT AUSTIN.
 Sousa, S. G., Alapini, A., Israelian, G., & Santos, N. C. 2010, A&A, 512, A13+
 Testa, P., Huenemoerder, D. P., Schulz, N. S., & Ishibashi, K. 2008, ApJ, 687, 579
 van den Ancker, M. E., de Winter, D., & Tjin A Djie, H. R. E. 1998, A&A, 330, 145
 van den Ancker, M. E., The, P. S., Tjin A Djie, H. R. E., et al. 1997, A&A, 324, L33
 Vick, M., Michaud, G., Richer, J., & Richard, O. 2011, A&A, 526, A37+
 Vigneron, C., Manganey, A., Catala, C., & Schatzman, E. 1990, Sol. Phys., 128, 287
 Vogt, S. S. & Penrod, G. D. 1983, ApJ, 275, 661
 Wade, G. A., Bagnulo, S., Drouin, D., Landstreet, J. D., & Monin, D. 2007, MNRAS, 376, 1145
 Waters, L. B. F. M. & Waelkens, C. 1998, ARA&A, 36, 233
 Zima, W. 2008, Communications in Asteroseismology, 155, 17
 Zima, W., Wright, D., Bentley, J., et al. 2006, A&A, 455, 235
 Zwintz, K. 2008, ApJ, 673, 1088
 Zwintz, K., Marconi, M., Kallinger, T., & Weiss, W. W. 2004, in IAU Symposium, Vol. 224, The A-Star Puzzle, ed. J. Zverko, J. Ziznovsky, S. J. Adelman, & W. W. Weiss, 353–358

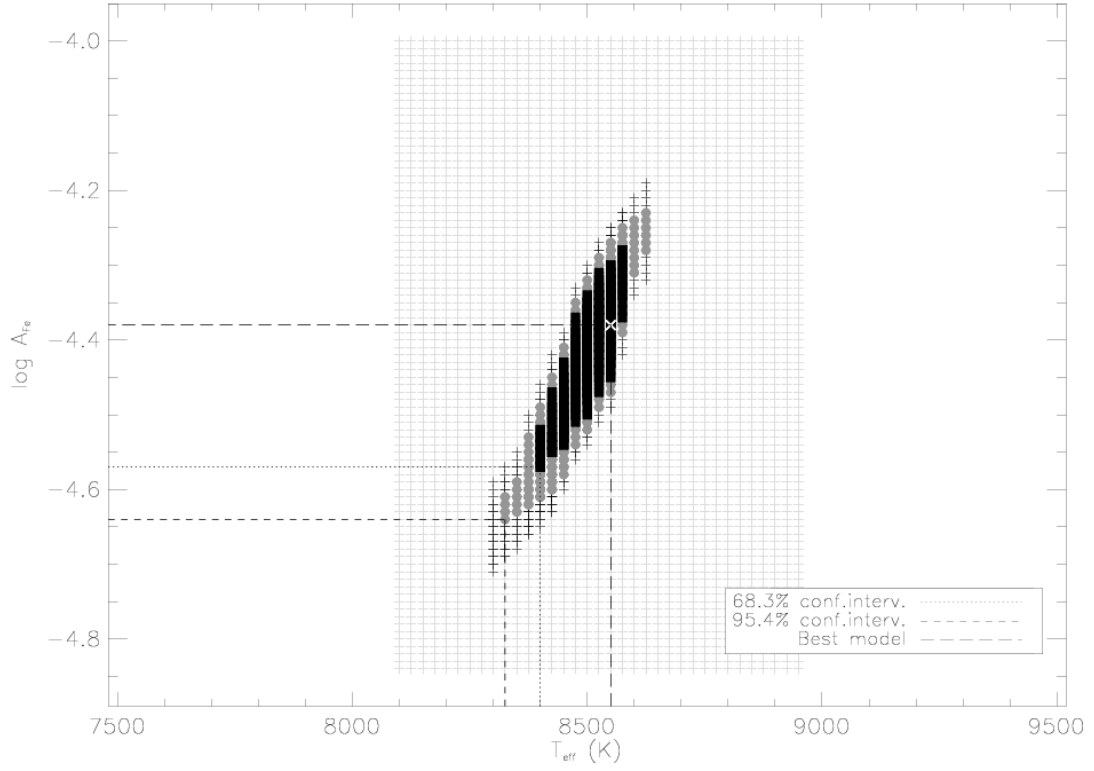


Fig. 9. 2D-repartition of the S_{red} values as a function of T_{eff} and $\log A_{\text{Fe}}$. The white X represents the best model, whose $T_{\text{eff}} = 8550$ K, $\log A_{\text{Fe}} = -4.38$ and $\log g = 3.9$. Confidence interval symbols are the same as those used in Fig. 7. Grey crosses have the same meaning as in Fig. 8.